Editors' Suggestion

Emergent multifractality in power-law decaying eigenstates

Adway Kumar Das [*] and Anandamohan Ghosh [†]
Indian Institute of Science Education and Research Kolkata, Mohanpur 741246, India

Ivan M. Khaymovich [‡]
Nordita, Stockholm University, and KTH Royal Institute of Technology, Hannes Alfvéns väg 12, SE-106 91 Stockholm, Sweden
and Institute for Physics of Microstructures, Russian Academy of Sciences, 603950 Nizhny Novgorod, GSP-105, Russia

(Received 4 February 2025; revised 17 June 2025; accepted 18 June 2025; published 1 July 2025)

Eigenstate multifractality is of significant interest with potential applications in various fields of quantum physics. Most of the previous studies concentrated on fine-tuned quantum models to realize multifractality, which is generally believed to be a critical phenomenon and fragile to random perturbations. In this work, we propose a set of generic principles based on the power-law decay of the eigenstates that allow us to distinguish a fractal phase from a genuine multifractal phase. We demonstrate the above principles in a 1D tight-binding model with inhomogeneous nearest-neighbor hopping that can be mapped to the standard quantum harmonic oscillator via energy-coordinate duality. We analytically calculate the fractal dimensions and the spectrum of fractal dimensions, which are in agreement with numerical simulations.

DOI: 10.1103/bnr3-5dcw

I. INTRODUCTION

Quantum ergodicity and its breakdown via emergent local integrals of motion are important for understanding the phenomenon of many-body localization (MBL) [1–8]. Despite being localized in real space, MBL eigenstates, as well as the ones in the monitored systems, simultaneously exhibit multifractality in the Hilbert space of dimension N, i.e., occupy an extensive volume $\propto N^D$ $(0 < D < 1)$ but a measure zero fraction of the entire Hilbert space [9–15]. Although widely observed in many-body systems, multifractality is rare in random-matrix models. It appears as a critical phenomenon at the Anderson localization transition [16–18] and in quasiperiodic systems [19–21], which are fragile to any uncorrelated disorder. The robust nonergodic extended phase in random-matrix models typically requires long-range coupling, e.g., the Rosenzweig-Porter model [22–40]. However, in all such models, the nonergodic phase hosts not multifractal but fractal states [41], characterized by the fractal dimension $D_q = D$ for all integers $q > 0$. In general, D_q dictates the scaling of the qth moments of wave-function intensity

$$\mathrm{I}_q = \sum_{\vec{n}} |\Psi_E(\vec{n})|^{2q} \sim N^{(1-q)D_q} \tag{1}$$

at energy E and the sum goes over the points $\vec{n}$ of a d-dimensional lattice of linear size L such that $N = L^d$.

In contrast to the fractal states, genuine multifractality is given by a nontrivial set of fractal dimensions $D_q > D_{q+1}$, $q \geqslant 1$, leading to many spatial and energy scales [17]. These multiple energy scales give multifractality potential applications in enhancing superconductivity [42–46], quantum algorithm speedups [47,48], and black hole physics [49–51]. Other than many-body systems, a robust multifractal phase exists only in the weighted adjacency matrices of random Erdös-Rényi graphs in a finite energy range [52–55]. In this paper, we discuss the main principles to realize genuine multifractal extended states in random matrices.

II. POWER-LAW DECAY AS A MECHANISM FOR MULTIFRACTALITY

Let us consider a generic d-dimensional system having eigenstates with a power-law decay

$$|\Psi_E(\vec{n}_0 + \vec{R})| \sim R^{-a}, \tag{2}$$

where the maximum intensity occurs at $\vec{n}_0$. For $d < 2a$, the normalization condition, $\mathrm{I}_1 = 1$ is dominated by a few lattice sites close to the location of the maximum intensity, $|\vec{n} - \vec{n}_0| \lesssim \mathcal{O}(1)$. Consequently, $D_q = 0$ for all integers $q \geqslant 1$ and the eigenstate is localized; see Fig. 1(a). The nonzero fractal dimensions appear only for $q < \frac{d}{2a} < 1$, which are determined by the wave-function tails, without affecting localization properties.

Even local perturbations of the localized states, keeping the power-law decaying tail at $|\vec{n} - \vec{n}_0| \gg \mathcal{O}(1)$ with $d < 2a$, can at most produce fractal states [56,57], as illustrated in Fig. 1(b). Since the maximum eigenstate intensity scales as $|\Psi_E(\vec{n}_0)|^2 \sim N^{-D_\infty}$ where $D_\infty \stackrel{\text{def}}{=} D_{q\to\infty}$ [58], for uncorrelated random local perturbation close to $\vec{n}_0$, the

[*]Contact author: akd19rs062@iiserkol.ac.in
[†]Contact author: anandamohan@iiserkol.ac.in
[‡]Contact author: ivan.khaymovich@gmail.com

Published by the American Physical Society under the terms of the Creative Commons Attribution 4.0 International license. Further distribution of this work must maintain attribution to the author(s) and the published article's title, journal citation, and DOI. Funded by Bibsam.

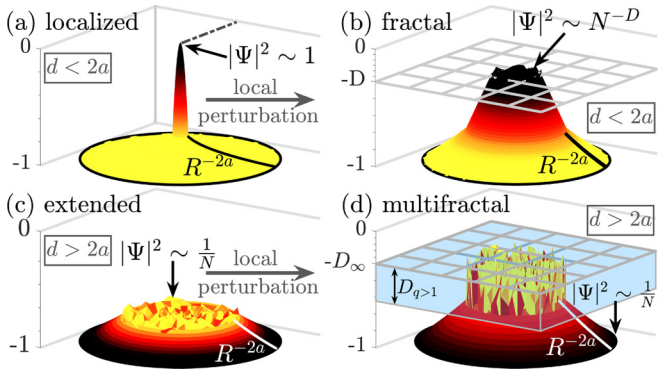


FIG. 1. Spatial structures of a d-dimensional power-law decaying wave function: (a) localized, (b) fractal, (c) extended, (d) multifractal. For (a) and (b), $|\Psi|^2 \sim \frac{1}{R^{2a>d}}$; for (c) and (d), $|\Psi|^2 \sim \frac{1}{R^{2a<d}}$. Dark colors signify the spatial regions mainly contributing to the normalization; the vertical axis shows $\ln|\Psi_E(\vec{n})|^2/\ln N$ with the maximum at $-D_\infty \stackrel{\text{def}}{=} \max_{\vec{n}} \ln|\Psi_E(\vec{n})|^2/\ln N$.

wave-function normalization condition implies that an $\mathcal{O}(N^{D_\infty})$ number of eigenstate intensities scale similarly to $|\Psi_E(\vec{n}_0)|^2$. Consequently, we get fractal states with $D_{q\geqslant 1} = D_\infty > 0$ as opposed to power-law localization in Fig. 1(a).

In the case of power-law decaying localized or fractal states with $d < 2a$, the normalization condition $\mathrm{I}_1 = 1$ is dominated by components around the maximum intensity. Contrarily for a slower decay, $d > 2a$, the normalization condition is dominated by the tail of the wave function, $|\vec{n} - \vec{n}_0| \sim \mathcal{O}(L)$, which contains $\mathcal{O}(N)$ typical (most probable) intensities, $|\Psi_{E,\mathrm{typ}}|^2 \sim N^{-1}$. In this case, the maximum intensity $|\Psi_E(\vec{n}_0)|^2 \sim N^{-D_\infty}$ barely contributes to the normalization; thus, D_∞ can take any value in $[0, 1]$. In particular, $D_\infty = 1$ corresponds to ergodicity, as shown in Fig. 1(c).

For a general value of D_∞, with a power-lay decaying wave function $|\Psi_E(\vec{n}_0 + \vec{R})| \simeq L^{a-d}R^{-a}$ and $q_* \stackrel{\text{def}}{=} \frac{d}{2a} > 1$, the state shows genuine multifractal properties [17], Fig. 1(d):

$$\mathrm{I}_q \simeq \sum_{\vec{R}} \left(\frac{L^{a-d}}{R^a}\right)^{2q} \sim N^{1-q} + \frac{N^{1-qD_\infty}}{N^{q_*(1-D_\infty)}}$$

$$\Leftrightarrow D_q = \begin{cases} 1, & q \leqslant q_* = \frac{d}{2a}, \\ 1 - (1 - D_\infty)\frac{q-q_*}{q-1}, & q > q_* > 1. \end{cases} \tag{3}$$

Such states are quite similar to those showing weak multifractality as recently found in random Erdös-Rényi graphs [52–55]. Thus, we identify the principle leading to genuine multifractality (fractality) for $d > 2a$ ($d < 2a$) as a manifestation of uncorrelated random local perturbations of power-law decaying states, which is one of the main results of this paper. In the definitions of [17] these states are genuinely multifractal, though this multifractality is dominated by the only monofractal wave-function support set $|\Psi_E(\vec{n})|^2 \sim |\Psi_E(\vec{n}_0)|^2 \sim N^{-D_\infty}$. In this sense, one can call this multifractality weak.

The simplest recipe to produce power-law decaying eigenstates in a tight-binding model with on-site disorder is to add power-law decaying hopping, e.g., dipolar Anderson [18,59–67] and random-matrix models [68–73]. But, spatial renormalization group [59–61] dictates that such perturbation breaks down at $a \leqslant d$ in long-range systems, yielding weak ergodicity for $\frac{d}{2} < a < d$ [74] and ergodicity at $a < \frac{d}{2}$ [75]. Only in the non-Hermitian setting, power-law decaying eigenstates can survive in the interval $\frac{d}{2} \leqslant a \leqslant d$ [76]. Therefore, long-range systems are unable to exhibit genuine multifractality, which requires $d > 2a$. Thus, we will focus on short-range 1D models with nearest-neighbor hopping having enough inhomogeneity to avoid exponential localization and will demonstrate that these are sufficient conditions to get genuine multifractality in power-law decaying eigenstates. This is the second important result in this paper.

Inhomogeneous nearest-neighbor hopping produces many interesting physics, e.g., Anderson localization [77–79], topological insulators [80,81], and perfect information transfer in pre-engineered quantum wires with parabolic hopping [82–85], which is experimentally realizable in photonic qubits [86]. Moreover, Lanczos reduction of many-body Hamiltonians in the Krylov basis [87–89] yields inhomogeneous tridiagonal matrices, where the growth of the correlated hopping elements dictates the transition from integrability to ergodicity [90].

The analogous uncorrelated case is represented by the well-known β ensemble [91], which is the Krylov-basis representation [92] of the Wigner-Dyson ensembles for Dyson index $\beta = 1$, 2, and 4 [93]. The β ensemble extends the Dyson index to any real number and shows many interesting properties: fractal eigenstates at the spectral edge [94] and in the bulk [95] coexisting with localized states without forming a mobility edge [96], or unusual long-range energy correlation [95,97,98] at $\beta \ll 1$. At the same time, power-law decay of the characteristic polynomials with nontrivial exponent $a = \frac{1}{4} + \frac{1}{2\beta}$ at large β values [99–102] may lead to the unusual eigenstate profile. Thus, the β ensemble should be an ideal candidate to produce genuine multifractality in power-law decaying eigenstates, at least for $\beta > 1$.

III. MEAN HAMILTONIAN

In this paper, we focus on the case $\beta \to \infty$ reducing to a deterministic tridiagonal *mean Hamiltonian*

$$\overline{H}_{m,n} = \sqrt{\frac{m}{2}}\delta_{m,n-1} + \sqrt{\frac{m-1}{2}}\delta_{m,n+1}. \tag{4}$$

The properties of $\overline{H}_{m,n}$ can be understood by a mapping to the quantum harmonic oscillator (QHO), $\hat{H}_Q = \frac{\hat{x}^2+\hat{p}^2}{2}$, where the nth eigenstate $|\Phi_n\rangle$ with energy $(n - \frac{1}{2})$ has the following real-space structure,

$$\Phi_n(x) = \pi^{-\frac{1}{4}} e^{-\frac{x^2}{2}} \frac{\mathcal{H}_{n-1}(x)}{\sqrt{2^{n-1}(n-1)!}}, \quad n \geqslant 1, \tag{5}$$

where $\mathcal{H}_n(x)$ is the nth-order Hermite polynomial [103]. The matrix element $\overline{H}_{m,n} = \langle\Phi_m|\hat{x}|\Phi_n\rangle$ of the position operator $\hat{x}$ in the eigenbasis ($\{|\Phi_n\rangle\}$) of $\hat{H}_Q$ leads to Eq. (4); thus, the energy axis of $\overline{H}_{m,n}$ maps to the spatial axis x of the QHO and vice versa, as shown in the top panel of Fig. 2. Hence, we denote the energy of the mean Hamiltonian, $\overline{H}_{m,n}$, as $E \stackrel{\text{def}}{=} x$ with eigenstates $|\Psi_x\rangle$. Imposing the open bound-

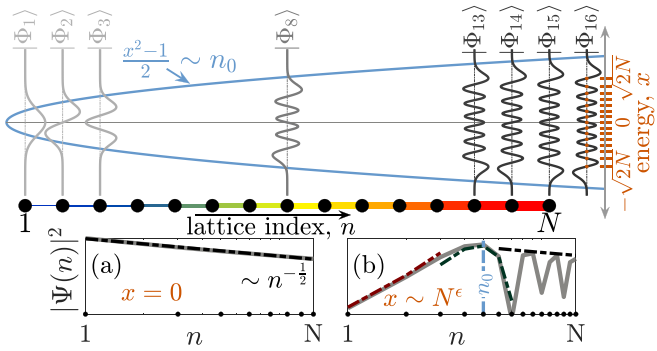


FIG. 2. QHO-to-mean-Hamiltonian correspondence: QHO eigenstates $|\Phi_n\rangle$ are plotted by gray lines inside the parabola $n = \frac{x^2-1}{2}$. The horizontal QHO energy axis corresponds to the real space $1 \leqslant n \leqslant N$ of $\overline{H}_{m,n}$. The eigenenergies of $\overline{H}_{m,n}$, given by the zeros of $\mathcal{H}_{15}$, lie on the vertical QHO coordinate axis. Color bar of increasing thickness in the n axis shows the $\sqrt{n}$ growth of the hopping terms. Eigenstate intensities of $\overline{H}_{m,n}$ (a) at $x = 0$, decay as $n^{-\frac{1}{2}}$; (b) in the spectral bulk $x \sim N^{\epsilon}$ (shown for $\epsilon = 0.3$), first, rapidly grow at $n \ll n_0$, Eq. (14), to the left of n_0, then have a smooth maximum Eq. (10) for $n \approx n_0$, followed by the power-law decay $\sim n^{-\frac{1}{2}}$ for $n \gg n_0 = \frac{x^2-1}{2}$, Eq. (15).

ary conditions, $\Psi_x(0) = 0$, $\Psi_x(N+1) = 0$, we obtain the recursive relation

$$\sqrt{n}\Psi_x(n) + \sqrt{n+1}\Psi_x(n+2) = \sqrt{2}x\Psi_x(n+1). \quad (6)$$

Thus, eigenstate components are given by the Hermite polynomials $\mathcal{H}_n(x)$,

$$\Psi_x(n) = \mathcal{Z}\frac{\mathcal{H}_{n-1}(x)}{\sqrt{2^{n-1}(n-1)!}}, \quad n = 1, 2, \ldots, N, \quad (7)$$

where $\mathcal{Z} \approx e^{-\frac{x^2}{2}}N^{-\frac{1}{4}}$ is the normalization factor (Appendix A), and the roles of the coordinate n and energy x are interchanged. The characteristics equation, $\det(H - x\mathbb{I}) = 0$, is resolved by x_j, the zeros of the Nth-order Hermite polynomial, $\mathcal{H}_N(x_j) = 0$, $1 \leqslant j \leqslant N$. The largest zero of $\mathcal{H}_N(x)$ is $\sqrt{2N} + \mathcal{O}(N^{-1/6})$ [104]; thus, the width of the density of states scales as $\mathcal{O}(\sqrt{2N})$ with the system size.

In order to characterize multifractality, similar to Eq. (1), we introduce the finite-size fractal dimensions $D_q^{(N)}$ via the qth moments of the wave-function intensity $|\Psi_x(n)|^2$ in the coordinate basis n,

$$\mathrm{I}_q^{(N)} = \sum_{n=1}^{N} |\Psi_x(n)|^{2q} \sim N^{(1-q)D_q^{(N)}}; \quad (8)$$

$\lim_{N\to\infty} D_q^{(N)} \equiv D_q$ is a monotonically decreasing function of q [105–107] bounded from below by D_∞. The latter gives the scaling of the maximum eigenstate intensity, $|\Psi_x(n_0)|^2 \sim N^{-D_\infty}$ [58], present at the spatial index

$$n \approx n_0 \equiv \frac{x^2-1}{2} \overset{\text{def}}{=} N^{2\epsilon}, \quad 0 \leqslant \epsilon \leqslant \frac{1}{2}, \quad (9)$$

given by the parabolic potential in QHO, Fig. 2. Upon increasing energy x (or ϵ), n_0 grows and approaches the system size N at the spectral edges $x \simeq \pm\sqrt{2N}$. This leads to the energy-dependent fractal dimensions D_q as we will now show via a systematic study of the system size scaling of the eigenstate intensities.

In order to obtain the eigenstate components near the maximum intensity, we approximate the Hermite polynomials in terms of Airy functions $\mathrm{Ai}(-y)$ (Appendix A), giving us

$$\Psi_x(n+1) \approx \frac{\mathrm{Ai}\left(-n_0^{-\frac{1}{3}}\eta\right)}{N^{\frac{1}{4}}n_0^{\frac{1}{12}}}, \quad \eta \equiv n - n_0 \ll n_0, \quad (10)$$

where $\mathrm{Ai}(-y)$ for an argument $y = n_0^{-\frac{1}{3}}\eta \sim \mathcal{O}(1)$ has a maximum value $\sim\mathcal{O}(1)$. For $y \gtrsim 1$, $\mathrm{Ai}(-y)$ decays as $\sim y^{-\frac{1}{4}}$ with oscillations as shown in Fig. 2(b). Hence, within $0 \leqslant y \lesssim 1$, equivalently within $1 \leqslant \eta \lesssim n_0^{\frac{1}{3}} \equiv N^{\frac{2\epsilon}{3}}$, we can consider $\mathrm{Ai}(-y)$ to be constant. Such an interval contains $\mathcal{O}(N^{\frac{2\epsilon}{3}})$ eigenstate intensities scaling similarly to the maximum intensity

$$|\Psi_x(n_0+\eta)|^2 \approx |\Psi_x(n_0)|^2 \approx N^{-\frac{1}{2}-\frac{\epsilon}{3}} \quad (11)$$

for a bulk state with energy $x \ll \sqrt{2N}$. Again, $|\Psi_x(n_0)|^2 \sim N^{-D_\infty}$ along with Eq. (11) implies that

$$D_\infty = \frac{1}{2} + \frac{\epsilon}{3}. \quad (12)$$

The fractal dimension D_∞ is energy dependent: At the center of the spectrum ($\epsilon = 0$), $D_\infty = \frac{1}{2}$, whereas $D_\infty = \frac{2}{3}$ for the spectral bulk, $\epsilon = \frac{1}{2}$. From Eq. (12), we get $D_\infty < 1$ implying that the bulk states must be at least nonergodic; i.e., they are not uniformly distributed in the $(N-1)$-dimensional unit hypersphere [58,108].

Next we need to determine whether the nonergodic bulk states of the mean Hamiltonian are fractal or multifractal. We can explicitly calculate all the fractal dimensions, D_q, or infer the multifractality from the spectrum of fractal dimensions (SFD), $f(\alpha)$ [17,109,110]. In a multifractal state, there are an $\mathcal{O}(N^{f(\alpha)})$ number of intensities that scale with the system size as $|\Psi|^2 \sim N^{-\alpha}$ for a range of $\alpha \geqslant 0$. The fractal dimension D_q is related to the SFD via the Legendre transform [17]

$$(q-1)D_q = \min_\alpha [q\alpha - f(\alpha)]. \quad (13)$$

Comparing with Eq. (12), we get $\alpha_{\min} = D_\infty$, while the number of such intensities is $N^{f(\alpha_{\min})}$ with $f(\alpha_{\min}) = \frac{2\epsilon}{3}$.

For $n \ll n_0$, there is a rapid monotonic growth of the eigenstate components with n (Appendix A), given by

$$\Psi_x(n+1) \approx \frac{e^{-\frac{x^2}{2}}}{(4\pi N)^{\frac{1}{4}}}x^{-\frac{1}{2}}\left(\frac{4x^2}{2n+1}\right)^{\frac{2n+1}{4}}. \quad (14)$$

Consequently, there are $\mathcal{O}(1)$ eigenstate components with arbitrarily small intensities for $n \ll n_0$, leading to $f(\alpha) = 0$ for large values of $\alpha \gg 1$ that do not contribute to D_q for $q > 0$ (Appendix A). We have ignored such α values for our subsequent calculation of the SFD.

On the right side of the maximum, $n \gg n_0$, we can approximate the eigenstate components at energy x as (Appendix A)

$$\Psi_x(n+1) \approx \left(\frac{2}{\pi N}\right)^{\frac{1}{4}}\frac{\cos\left(\frac{n\pi}{2} - \sqrt{2n+1}x\right)}{n^{\frac{1}{4}}}. \quad (15)$$

Hence, eigenstate intensities oscillate with an envelope decaying as $n^{-\frac{1}{2}}$; see Fig. 2(b). In agreement with our principle of observing genuine multifractality in power-law decaying states, the bulk states of the mean Hamiltonian exhibit the power-law decay n^{-2a} with the exponent $2a = \frac{1}{2} < d$.

Now we calculate the entire SFD for the bulk eigenstates of the mean Hamiltonian. In Eq. (15), the cosine part has a magnitude of order 1 for most of the values of $n \gg n_0$. First, we consider the scaling of the envelope where the intensities $|\Psi_x(n+1)|^2 \sim (nN)^{-\frac{1}{2}} \sim N^{-\alpha}$. The number of such components is $n - n_0 \sim n \sim N^{f(\alpha)}$, implying that

$$\alpha = \frac{1}{2} + \frac{f(\alpha)}{2} \Rightarrow f(\alpha) = 2\alpha - 1. \tag{16}$$

It now remains to determine the bounds on the exponent α. The upper bound can be obtained by substituting $n \sim N$ in Eq. (15). In this limit, i.e., at the tail, $\mathcal{O}(N)$ eigenstate intensities scale as N^{-1}, leading to $f(\alpha) = 1$ at $\alpha = 1$. On the other hand, in order to obtain the lower bound, we consider the scaling of the energy as $n_0 \sim N^{2\epsilon}$, $n \gg n_0$, and $n \sim N^{f(\alpha)}$. It is easy to see that $f(\alpha) > 2\epsilon$, leading to the lower bound $\alpha > \frac{1}{2} + \epsilon$. The lower bound can be further refined by considering Eq. (10), which also implies the same power-law decay at $n - n_0 \equiv \eta \gg n_0^{\frac{1}{3}}$, leading to $f(\alpha) = 2\alpha - 1$ with a left bound on α given by $\eta \sim N^{f(\alpha)} \gg n_0^{\frac{1}{3}} \Leftrightarrow \alpha > \frac{2\epsilon}{3}$. Therefore, the power-law decaying envelope of the bulk states for $n \gtrsim n_0$ at energy $x \sim N^{\epsilon}$ leads to the following SFD:

$$f(\alpha) = 2\alpha - 1, \quad \frac{1}{2} + \frac{\epsilon}{3} \leqslant \alpha \leqslant 1. \tag{17}$$

Now we consider the small cosine values in Eq. (15) corresponding to atypically small wave-function components and obtain the full SFD even for $\alpha > 1$. The zeros of the cosine part in Eq. (15) reside at the lattice indices $n_0 \lesssim n_k \leqslant N$ such that $\sqrt{2n_k + 1}x \approx k\pi$ for odd n_k and $\sqrt{2n_k + 1}x \approx k\pi + \frac{\pi}{2}$ for even n_k. We focus only on the odd values of n_k, as the even case is fully analogous. Since $n_0 \approx x^2 = N^{2\epsilon}$ and $n_k \approx \frac{\pi^2 k^2}{x^2}$, we get

$$x^2 \lesssim k \leqslant \sqrt{N}x. \tag{18}$$

For small deviations $\delta_n = |n - n_k|$, we can approximate the cosine as

$$(\sqrt{n_k + \delta_n} - \sqrt{n_k})x \sim \frac{x\delta_n}{\sqrt{n_k}} \ll 1. \tag{19}$$

Then, intensities scale as $N^{-\alpha} \sim (Nn_k)^{-\frac{1}{2}}(\frac{x\delta_n}{\sqrt{n_k}})^2$ within the interval $[n_k - \delta_n, n_k + \delta_n]$. As there are k zeros of Eq. (15), present up to $n = n_k$, there are $k\delta_n \sim N^{f(\alpha)}$ components with intensity $\sim N^{-\alpha}$. Substituting δ_n from one expression to another and taking into account that $\sqrt{n_k}x \sim k$, one finds that

$$f(\alpha) = \frac{1}{4} - \frac{\alpha}{2} + \frac{5}{2}\frac{\ln\frac{k}{x}}{\ln N}. \tag{20}$$

Equation (20) is dominated by the maximum value of $k = \sqrt{N}x$, Eq. (18). Therefore, the atypically small intensities of the bulk states for $n \gtrsim n_0$ at energy $x \sim N^{\epsilon}$ produce the SFD

$$f(\alpha) = \frac{3 - \alpha}{2}, \quad 1 \leqslant \alpha. \tag{21}$$

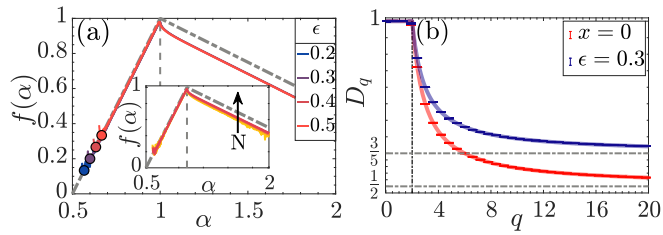


FIG. 3. Multifractality of bulk states: (a) Spectrum of fractal dimensions for several energies $x = N^{\epsilon}$ for $N = 10^9$. The markers denote $\alpha_{\min} = \frac{1}{2} + \frac{\epsilon}{3}$ and the dashed line denotes the analytical expressions from Eqs. (17) and (21). The inset shows $f(\alpha)$ for $\epsilon = 0.3$ and different N from 10^6 to 10^9. (b) Fractal dimensions, D_q, vs q at energies $x = 0$ and $x = N^{0.3}$. Solid lines denote analytical expression from Eq. (22) and horizontal dashed lines denote D_∞ from Eq. (12).

In Fig. 3(a), we show the numerical estimate of the entire SFD for different N and ϵ, giving an excellent agreement with Eqs. (17) and (21).

The Legendre transform, Eq. (13), of $f(\alpha)$ from Eqs. (17) and (21) gives the fractal dimensions

$$D_q = \begin{cases} 1, & 0 \leqslant q \leqslant 2, \\ 1 - \left(\frac{1}{2} - \frac{\epsilon}{3}\right)\frac{q-2}{q-1}, & q > 2, \end{cases} \tag{22}$$

which is in the full agreement with our generic result Eq. (3) for $a = \frac{1}{4}$ and $d = 1$. The limit $q \to \infty$ in the above expression retrieves D_∞ given in Eq. (12). In Fig. 3(b), the numerically estimated D_q versus q for eigenstates at energies $x \sim N^{0.3}$ and $x = 0$ show excellent agreement with the analytical expression from Eq. (22). Importantly we show the q dependence of D_q implying multifractality in the eigenstate fluctuations.

IV. ROBUSTNESS OF THE MULTIFRACTALITY OF THE MEAN HAMILTONIAN

In this section, we show that the multifractality observed in the bulk energy spectrum of the mean Hamiltonian, $\overline{H}$, is not a fine-tuned property, rather robust against even nonlocal perturbations (which introduce long-range hopping). Recall that $|\Psi_x\rangle$, the bulk energy eigenstate of $\overline{H}$ at energy $x = N^{\epsilon}$, is multifractal with an almost flat head (envelope of equal intensities) consisting of an $\mathcal{O}(N^{\frac{2\epsilon}{3}})$ number of components centered around the lattice site $n_0 \sim N^{2\epsilon}$. On the left side of such a flat head, the eigenstate components decay faster than exponential, so we can effectively ignore them. On the right side of the eigenstate head, a power-law decaying tail is present such that $\mathcal{O}(N)$ components on the right edge of the lattice behave similarly to those of an ergodic state [i.e., equal intensities $\sim\mathcal{O}(N^{-1})$].

From the above discussion, we see that the energy eigenstate $|\Psi_x\rangle$ at energy $x \sim N^{\epsilon}$ has negligibly small components over the lattice sites $n < N^{2\epsilon} - N^{\frac{2\epsilon}{3}}$. So, intuitively we expect $|\Psi_x\rangle$ to be effectively protected against perturbations over lattice sites $n < N^{2\epsilon} - N^{\frac{2\epsilon}{3}}$. Moreover, if a nonlocal perturbation centered around the lattice site $n_0 \sim N^{2\epsilon}$ has a range M smaller than the size of eigenstate head, then such a perturbation cannot hybridize $|\Psi_x\rangle$ with other energy states at different

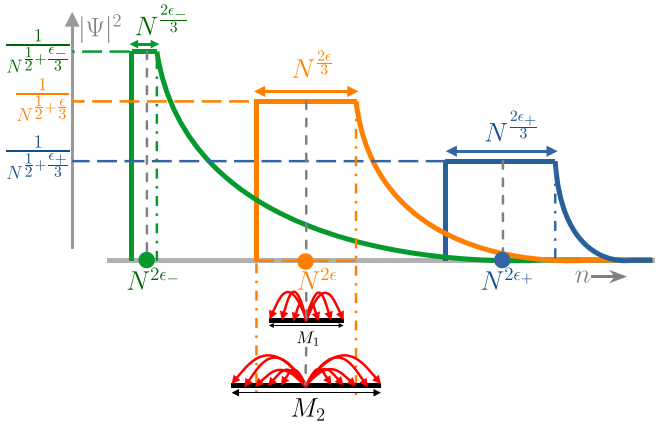


FIG. 4. Approximate intensity profile of the eigenstates of the mean Hamiltonian, $\overline{H}$, over lattice space at different energies, $x = N^{\epsilon}$, where $0 < \epsilon_- < \epsilon < \epsilon_+ < 1/2$. The nonlocal perturbation has range M while the unperturbed Hamiltonian had only nearest-neighbor hopping. The multifractality from $\overline{H}$ remains unperturbed for $M_1 < N^{\frac{2\epsilon}{3}}$, where $N^{\frac{2\epsilon}{3}}$ is the size of the eigenstate head. As $M_2 > N^{\frac{2\epsilon}{3}}$, eigenstates at different energy scales hybridize and alter the spectrum of fractal dimensions.

energy scales, $\epsilon' \neq \epsilon$. The hybridization of the states around the energy $x \sim N^{2\epsilon}$ does not change their fractal dimensions as they live at the same multifractal support. Thus, even if we introduce long-range hopping over M sites around $n_0 \sim N^{\epsilon}$, the multifractal structure of $|\Psi_x\rangle$ should be robust provided $M < N^{\frac{2\epsilon}{3}}$. This is schematically explained in Fig. 4.

To test the above idea, we perturb an $N \times N$ mean Hamiltonian $\overline{H}$ with a random matrix H_0,

$$H = \overline{H} + \lambda H_0, \quad H_0 = \mathbb{P} H_{\mathrm{GOE}} \mathbb{P},$$
$$\mathbb{P} = \sum_{|n-n_0| \leqslant \lfloor \frac{M}{2} \rfloor} |n\rangle \langle n|, \quad M = \lfloor N^{\eta} \rfloor,$$
$$n_0 = \lfloor N^{2\epsilon_0} \rfloor, \quad \lambda = N^{-\zeta}, \tag{23}$$

where λ controls the strength of the perturbation, H_{GOE} is an $N \times N$ Gaussian orthogonal ensemble (GOE) matrix, and $\mathbb{P}$ is a projection operator over the site basis, $\{|n\rangle\}$. Thus, varying $M \sim N^{\eta}$ and $n_0 \sim N^{\epsilon_0}$, we can control the range and location of perturbation, respectively. $\mathbb{P} H_{\mathrm{GOE}} \mathbb{P}$ is an $M \times M$ GOE matrix with an energy bandwidth $\mathcal{O}(\sqrt{M})$. Such a perturbation introduces diagonal disorder $\sim \mathcal{O}(1)$ in the lattice sites within the spatial window $[n_0 - \lfloor \frac{M}{2} \rfloor, n_0 + \lfloor \frac{M}{2} \rfloor]$ and random hopping with range M around the lattice site n_0.

In Eq. (23), we vary the free parameters as a power of the system size as $\overline{H}$ has an energy bandwidth $\mathcal{O}(\sqrt{N})$. Therefore, η, ϵ_0, and ζ control the range, location, and strength of the random perturbation, respectively. In particular, the location of the perturbation introduces the energy scale $x = N^{\epsilon_0}$ such that for highly nonlocal perturbation $M > N^{\frac{2\epsilon_0}{3}}$, two possibilities arise:

(i) $\epsilon > \epsilon_0$: corresponding energy states are robust against the perturbation;

(ii) $\epsilon \leqslant \epsilon_0$: sufficiently strong perturbation can lead to hybridization, altering the fractal structures.

In the rest of the discussion, we fix $\epsilon_0 = 0.3$; i.e., the perturbation is added around the lattice site $\lfloor N^{0.6} \rfloor$. To understand the multifractality in the perturbed Hamiltonian, we need to compute the fractal dimensions D_q by extrapolating finite-size fractal dimensions $D_q^{(N)}$ with respect to the system sizes. However, for nonlocal perturbation, $D_q^{(N)}$ can be computed using exact diagonalization, which does not allow access to large system sizes. On the other hand, $D_q^{(N)}$ shows a strong finite-size effect for $q \gg 1$. Thus, we look at the scaled fractal dimension

$$\tilde{D}_q \equiv \frac{D_q^{(N)}}{D_q^{(N,\mathrm{GOE})}}, \tag{24}$$

which converges to unity for an ergodic state. Note that the nonmonotonicity of $\tilde{D}_q$ versus q is given by the nontrivial q dependence of the ergodic $D_q^{(N,\mathrm{GOE})}$ and is not related to any violation of the monotonicity of $D_q^{(N)}$ itself.

In Fig. 5[I], we consider the perturbed Hamiltonian from Eq. (23) for $N = 4097$ and show the ensemble-averaged scaled fractal dimensions of the eigenstates at various energies $x = N^{\epsilon}$ while varying the perturbation strength, $\lambda = N^{-\zeta}$.

Local perturbation: For $\eta = 0$, the range of perturbation, M is $\mathcal{O}(1)$, hence, local (in the simulation, we take $M = 3$). We find that the fractal dimensions are the same as those from the mean Hamiltonian irrespective of the choice of energy and strength of perturbation; see Fig. 5[I], panels (a)–(d). This follows our expectation from Fig. 4, which implies that a flat eigenstate head spanning over an extensive number of lattice sites $[\sim \mathcal{O}(N^{\frac{2\epsilon}{3}})]$ cannot be destroyed by a local perturbation at $n_0 \gg 1$, i.e., $\epsilon_0 > 0$.

Nonlocal perturbation: If $\eta > 0$, then, $M = \lfloor N^{\eta} \rfloor$, the effective dimension of the perturbing Hamiltonian is an extensive number, hence, the perturbation becomes nonlocal. In particular, for $\eta \sim \frac{2\epsilon_0}{3}$, the range of perturbation is similar to one of the unperturbed eigenstate heads. Then, a sufficiently strong perturbation can destroy the multifractality at energy $x = N^{\epsilon_0}$, as shown in Fig. 5[I](g).

The eigenstates of $\overline{H}$ at energy $x \sim N^{\epsilon}$ with $\epsilon_0 < \epsilon$ have a flat head centered around $N^{2\epsilon}$ and negligibly small components over the lattice sites $n < N^{2\epsilon} - N^{\frac{2\epsilon}{3}} \approx N^{2\epsilon}$. As $N^{2\epsilon_0} < N^{2\epsilon}$ for $\epsilon_0 < \epsilon$, the eigenstate with energy $x \sim N^{\epsilon}$ is effectively decoupled from the lattice sites $n < n_0$. Hence, even an extensively long-range perturbation with $0 < \eta \leqslant \frac{2\epsilon_0}{3}$ cannot change the fractal dimensions at the energy $x \sim N^{\epsilon}$ with respect to $\overline{H}$, as shown in Fig. 5[I](h). For example, if $\epsilon_0 = 0$, both η and $n_0 \sim \mathcal{O}(1)$ and we add a local perturbation to the left edge of the lattice. In this case, the spectral structure remains unchanged at any extensive bulk energy [$\epsilon > 0$; see Fig. 5[II], panels (b)–(d)].

At the same time at $\epsilon_0 > \epsilon$ the overlap of the eigenfunctions with the ones at $x \sim N^{\epsilon_0}$, resonant to the above perturbation, is diminished by the power-law decay of their tails, thus, showing small deviations in Fig. 5[I], panels (e) and (f), for the range of the perturbation amplitudes $\lambda \sim N^{-\zeta}$.

To sum up, for the critical value of $M \sim N^{\frac{2\epsilon_0}{3}}$, only the resonant states close to $x \sim N^{\epsilon_0}$ are significantly affected.

Nonlocal perturbation with range larger than the eigenstate head: For $\eta > \frac{2\epsilon_0}{3}$, the range of perturbation exceeds the length of the eigenstate head at energy $x = N^{\epsilon_0}$, leading

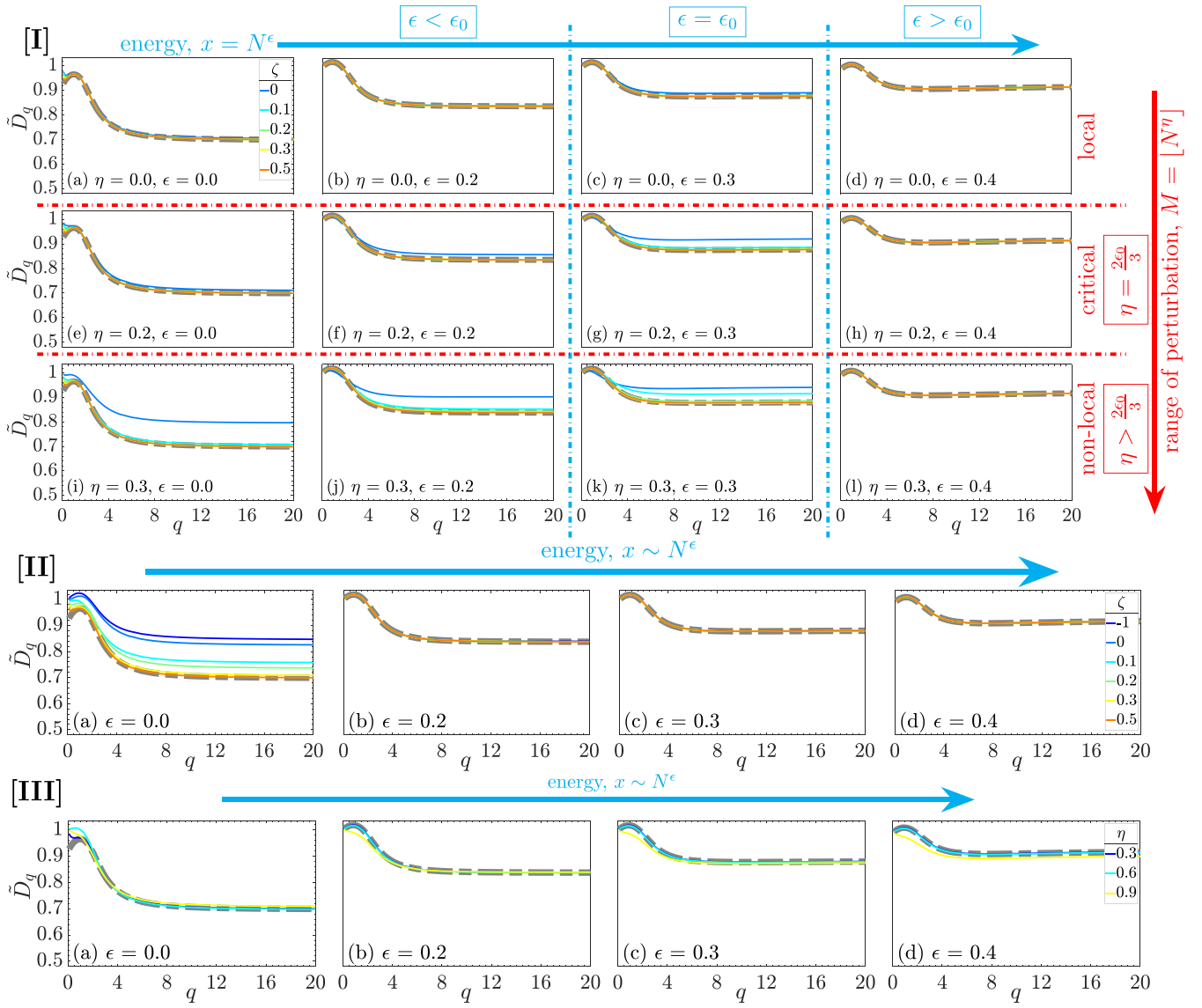


FIG. 5. [I] Scaled fractal dimension vs q for the perturbed Hamiltonian in Eq. (23) at different energies, N^{ϵ}, with $N = 4097$, and various values of $M \sim N^{\eta}$ (range of perturbation), ϵ (energy scale), and $\lambda \sim N^{\zeta}$ (strength of perturbation; given in legend). The perturbation is added around the lattice site $n_0 = \lfloor N^{2\epsilon_0} \rfloor$ and we take $\epsilon_0 = 0.3$. The gray dashed line denotes the finite-size fractal dimensions of the mean Hamiltonian. Data averaged over 128 disorder realizations and normalized by the finite-size fractal dimensions of the GOE. [II] Local perturbation at the left edge of the lattice: scaled fractal dimensions for H [Eq. (23)] at different energies, N^{ϵ}, with $N = 4097$, $n_0 = 2$, $M = 3$, and various values of ζ (strength of perturbation; given in legend). The blue (gray) dashed line denotes the finite-size fractal dimensions of GOE (mean Hamiltonian). Data averaged over 128 disorder realizations. [III] Extensively long-range perturbation at the right edge of the lattice: scaled fractal dimensions for H [Eq. (23)] at different energies, N^{ϵ}, with $N = 4097$, $\lambda = 1$, and various values of η (range of perturbation; given in legend). The blue (gray) dashed line denotes the finite-size fractal dimensions of GOE (mean Hamiltonian). Data averaged over 128 disorder realizations.

to the hybridization of eigenstates at different energy scales. Consequently, the fractal dimensions increase, thus gradually destroying the multifractal structure of the mean Hamiltonian at energies smaller than N^{ϵ_0}, as shown in Fig. 5[I], panels (i)–(k). However, eigenstates at larger energies remain unperturbed, as seen in Fig. 5[I](l).

The bulk eigenstates of the mean Hamiltonian have $\mathcal{O}(N)$ intensities of strength $\mathcal{O}(N^{-1})$ (similar to an ergodic state) present at the tail of the state, spanning an extensively large number of lattice sites at the right edge of the lattice. We find that this spatial region is unexpectedly robust against extensively long-range perturbations ($\eta > 0$), as shown in Fig. 5[III].

In Fig. 6, we show the finite-size fractal dimension for $q = 10$ as a function of the range of perturbation at various energies. Such a plot shows that the fractal dimensions remain unchanged as long as the range of perturbation is smaller than the eigenstate head size at the location of perturbation, i.e., $\eta < \frac{2\epsilon_0}{3}$. Figure 6 also shows that for highly nonlocal perturbation, $\eta > \frac{2\epsilon_0}{3}$, fractal structure is robust at energy scale $\epsilon > \epsilon_0$.

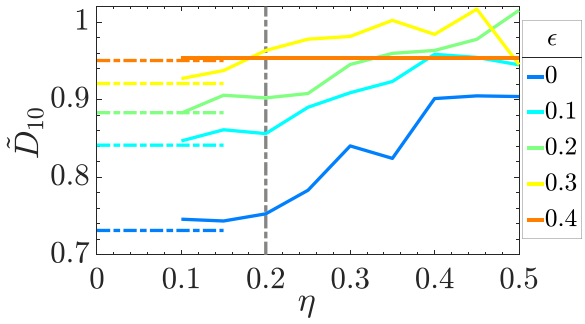


FIG. 6. Scaled fractal dimension at $q = 10$ vs the range of perturbation (effective size of the perturbing Hamiltonian, $M = \lfloor N^{\eta} \rfloor$) at various energies ($x = N^{\epsilon}$) for $N = 4097$, $\epsilon_0 = 0.3$, and $\lambda = 1$ (i.e., $\zeta = 0$). Horizontal dashed lines denote the fractal dimension of the mean Hamiltonian.

In summation, we show that depending on the location of the perturbation, even nonlocal disordered perturbations cannot destroy the multifractality present in the bulk spectrum of the mean Hamiltonian.

V. CONCLUSION

To summarize, in this paper, we provide a simple but powerful principle to realize genuine multifractality as a quantum phase. The necessary criteria for such a phase is to have a sufficiently slow power-law decay of the eigenstates with an exponent at least two times smaller than the lattice dimensionality. We discuss why in most of the long-range models such wave-function power-law decay cannot be realized and only fractal phases of matter can be observed. As an illustration of our principle, we provide a short-range 1D Hamiltonian where genuine multifractal states with the power-law decaying profile are realized and analytically find their fractal dimensions. As the considered model is the $\beta \to \infty$ limit of the β ensemble, we expect that predicted multifractality will survive for finite $\beta > 1$ at least until the eigenstates localize [99,100], but we keep the detailed investigation of these cases for our future studies. One should note that the above principle of the power-law wave-function decay with the power smaller than the dimensionality of the lattice can be straightforwardly generalized to the exponential decay on the hierarchical graphs, where the number of neighbors also grows exponentially with the distance. Indeed, if the corresponding exponential wave-function decay is smaller than the one of the exponential growth of the site number with the distance R from a certain site, then the same arguments of normalization, as in Fig. 1, are applicable and can explain the results of the recent papers on such graphs [52–55]. On the other hand, the above papers demonstrate additional examples of multifractality and applicability of the principle suggested in our paper.

ACKNOWLEDGMENTS

A.K.D. is supported by an INSPIRE Fellowship, DST, India, and Fulbright-Nehru Grant No. 2879/FNDR/2023-2024. I.M.K. acknowledges the support of the European Research Council under the European Union's Seventh Framework Program Synergy ERC-2018-SyG HERO-810451.

DATA AVAILABILITY

The data that support the findings of this article are not publicly available. The data are available from the authors upon reasonable request.

APPENDIX A: ASYMPTOTES OF THE HERMITE POLYNOMIALS AND EIGENSTATE COMPONENTS OF MEAN HAMILTONIAN

Following the approximation of Hermite polynomials [104,111], the eigenstate components of the mean Hamiltonian at energy x can be expressed as

$$\Psi_x(n+1) \approx \begin{cases} C_x n^{-\frac{1}{4}} \left(\frac{x^2}{2n+1} - 1\right)^{-\frac{1}{4}} e^{(n+\frac{1}{2})(\cosh^{-1}\frac{x}{\sqrt{2n+1}} - \frac{x}{\sqrt{2n+1}}\sqrt{\frac{x^2}{2n+1}-1})}, & n < n_0, \\ \frac{\mathcal{Z}(2\pi)^{\frac{1}{4}}}{n^{\frac{1}{12}}} e^{\sqrt{2n}x - n} \mathrm{Ai}(\sqrt{2}(x - \sqrt{2n}) n^{\frac{1}{6}}), & n \approx n_0, \\ C_x n^{-\frac{1}{4}} \left(1 - \frac{x^2}{2n+1}\right)^{-\frac{1}{4}} \sin\left(\frac{3\pi}{4} + \left(n+\frac{1}{2}\right)\left(\frac{x}{\sqrt{2n+1}}\sqrt{1 - \frac{x^2}{2n+1}} - \cos^{-1}\frac{x}{\sqrt{2n+1}}\right)\right), & n > n_0, \end{cases} \tag{A1}$$

where $n_0 \equiv \frac{x^2-1}{2}$, $C_x = \frac{\mathcal{Z} e^{\frac{x^2}{2}}}{(8\pi)^{\frac{1}{4}}}$ if $n < n_0$, and $C_x = \frac{\mathcal{Z} e^{\frac{x^2}{2}}}{(\pi/2)^{\frac{1}{4}}}$ otherwise, and $\mathcal{Z}$ is the eigenstate normalization factor.

1. Eigenstate components for $n \ll n_0$

Equation (A1) implies that for $n \ll n_0$,

$$\Psi_x(n+1) \approx C_x n^{-\frac{1}{4}} \frac{(2n+1)^{\frac{1}{4}}}{\sqrt{x}} \exp\left(\left(n+\frac{1}{2}\right)\left(\cosh^{-1}\frac{x}{\sqrt{2n+1}} - \frac{x}{\sqrt{2n+1}}\sqrt{\frac{x^2}{2n+1}-1}\right)\right)$$
$$\approx \frac{C_x}{\sqrt{x}} n^{-\frac{1}{4}} (2n+1)^{\frac{1}{4}} \exp\left(\left(n+\frac{1}{2}\right)\left(\ln\frac{2x}{\sqrt{2n+1}} - \frac{x^2}{2n+1}\right)\right)$$

$$= \frac{C_x}{\sqrt{x}} n^{-\frac{1}{4}} (2n+1)^{\frac{1}{4}} \left(e^{-\frac{x^2}{2n+1}} \frac{2x}{\sqrt{2n+1}} \right)^{n+\frac{1}{2}} = \frac{C_x}{\sqrt{x}} e^{-\frac{x^2}{2}} \frac{(2x)^{n+\frac{1}{2}}}{n^{\frac{1}{4}}(2n+1)^{\frac{n}{2}}} = \frac{\mathcal{Z} e^{\frac{x^2}{2}}}{(8\pi)^{\frac{1}{4}}\sqrt{x}} e^{-\frac{x^2}{2}} \frac{(2x)^{n+\frac{1}{2}}}{n^{\frac{1}{4}}(2n+1)^{\frac{n}{2}}}$$

$$\Rightarrow \Psi_x(n+1) \approx \frac{\mathcal{Z}}{(4\pi)^{\frac{1}{4}}} x^{-\frac{1}{2}} \left(\frac{4x^2}{2n+1} \right)^{\frac{2n+1}{4}}. \tag{A2}$$

Since $\frac{x^2}{2n+1} \gg 1$, $\Psi_x(n+1)$ is a monotonically increasing function of n for $n \ll n_0$.

2. Eigenstate components for $n \gg n_0$

Let $m = \frac{x}{\sqrt{2n+1}}$. Then, for $n \gg n_0$ (where $C_x = \frac{\mathcal{Z} e^{\frac{x^2}{2}}}{(\pi/2)^{\frac{1}{4}}}$),

$$\begin{aligned}
\Psi_x(n+1) &\approx C_x n^{-\frac{1}{4}} (1-m^2)^{-\frac{1}{4}} \cos\left(\frac{\pi}{4} + \left(n+\frac{1}{2}\right)(m(1-m^2)^{\frac{1}{2}} - \cos^{-1} m) \right) \\
&\approx C_x n^{-\frac{1}{4}} \left(1 + \frac{m^2}{4}\right) \cos\left(\frac{\pi}{4} + \left(n+\frac{1}{2}\right)\left(m - \frac{m^3}{2} - \frac{\pi}{2} + m + \frac{m^3}{6} \right) \right) \\
&\approx C_x n^{-\frac{1}{4}} \cos\left(-\frac{n\pi}{2} + m(2n+1) \right) \approx \begin{cases} (-1)^m C_x n^{-\frac{1}{4}} \cos(\sqrt{2n+1}x), & n = 2m, \\ (-1)^m C_x n^{-\frac{1}{4}} \sin(\sqrt{2n+1}x), & n = 2m+1. \end{cases}
\end{aligned} \tag{A3}$$

Therefore, the eigenstate components oscillate and the envelope decays as $n^{-\frac{1}{4}}$ for $n \gg n_0$.

3. Normalization constant of the eigenstate

As the eigenstate components monotonically increase for $n \ll n_0$ and decay as $n^{-\frac{1}{4}}$ for $n \gg n_0$, the maximum intensity occurs at $n = n_0 \approx \frac{x^2-1}{2}$. If we take a bulk energy $x \ll \sqrt{2N}$, then

$$\sum_{n=0}^{N-1} |\Psi_x(n+1)|^2 \approx \frac{\mathcal{Z}^2 e^{x^2}}{\sqrt{\pi/2}} \sum_{n=n_0+1}^{N-1} n^{-\frac{1}{2}} \approx \frac{\mathcal{Z}^2 e^{x^2}}{\sqrt{\pi/2}} \left(h\left(N-1, \frac{1}{2}\right) - h\left(n_0, \frac{1}{2}\right) \right) \approx \frac{\mathcal{Z}^2 e^{x^2}}{\sqrt{\pi/2}} 2(\sqrt{N} - \sqrt{n_0}) \Rightarrow \mathcal{Z} \approx e^{-\frac{x^2}{2}} N^{-\frac{1}{4}}, \tag{A4}$$

where $\zeta(x)$ is the Riemann zeta function and $h(n, r) = n$th harmonic number of order r approximated using the Euler-Maclaurin sum formula [$h(n, \frac{1}{2}) = \zeta(\frac{1}{2}) + 2\sqrt{n} + \mathcal{O}(n^{-\frac{1}{2}})$].

4. Eigenstate components around the maximum intensity

Following the approximation of the Hermite polynomials for $x \to \sqrt{2n}$ and $n \to \infty$ [111], we get

$$\Psi_x(n+1) = (2\pi)^{\frac{1}{4}} N^{-\frac{1}{4}} n^{-\frac{1}{12}} \exp\left(\sqrt{2n}x - n - \frac{x^2}{2} \right) \mathrm{Ai}(\sqrt{2}(x - \sqrt{2n}) n^{\frac{1}{6}}), \tag{A5}$$

where $\mathrm{Ai}(y)$ is the Airy function. Let, $n = n_0 + \eta$, $\eta \ll n_0$, such that the approximation in Eq. (A5) is valid for $n_0 \lessapprox n \lessapprox n_0 + \eta$. Then, we can simplify Eq. (A5) as

$$\begin{aligned}
\Psi_x(n+1) &\approx N^{-\frac{1}{4}} (n_0+\eta)^{-\frac{1}{12}} \exp\left(\sqrt{2(n_0+\eta)}x - (n_0+\eta) - \frac{x^2}{2} \right) \mathrm{Ai}(\sqrt{2}[x - \sqrt{2(n_0+\eta)}](n_0+\eta)^{\frac{1}{6}}) \\
&\approx N^{-\frac{1}{4}} n_0^{-\frac{1}{12}} \exp\left(2n_0\left(1 + \frac{\eta}{2n_0}\right) - 2n_0 - \eta \right) \mathrm{Ai}\left(2\sqrt{n_0}\left(1 - \sqrt{1 + \frac{\eta}{n_0}}\right) n_0^{\frac{1}{6}} \left(1 + \frac{\eta}{n_0}\right)^{\frac{1}{6}} \right) \\
&\approx N^{-\frac{1}{4}} n_0^{-\frac{1}{12}} \mathrm{Ai}(-n_0^{-\frac{1}{3}}\eta).
\end{aligned} \tag{A6}$$

Combining Eqs. (A2), (A3), and (A6) we get

$$\Psi_x(n+1) \approx \begin{cases} \frac{e^{-\frac{x^2}{2}}}{(4\pi N)^{\frac{1}{4}}} x^{-\frac{1}{2}} \left(\frac{4x^2}{2n+1}\right)^{\frac{2n+1}{4}}, & n \ll n_0, \\ N^{-\frac{1}{4}} n_0^{-\frac{1}{12}} \mathrm{Ai}(-n_0^{-\frac{1}{3}}\eta), & n \approx n_0, \\ \left(\frac{2}{\pi N}\right)^{\frac{1}{4}} n^{-\frac{1}{4}} \cos\left(\frac{n\pi}{2} - \sqrt{2n+1}x\right), & n \gg n_0. \end{cases} \tag{A7}$$

5. Spectrum of fractal dimensions for $n \gg n_0$

Equation (A2) implies that for $n \ll n_0$

$$\Psi_x(n+1) \approx \frac{N^{-\frac{1}{4}} e^{-\frac{x^2}{2}}}{(4\pi)^{\frac{1}{4}}} x^{-\frac{1}{2}} \left(\frac{4x^2}{2n+1}\right)^{\frac{2n+1}{4}}$$

$$\Rightarrow N^{-\alpha} = N^{-\frac{1}{2}} e^{-x^2} x^{-1} \left(\frac{4x^2}{2n+1}\right)^{\frac{2n+1}{2}} = N^{-\frac{1}{2}} e^{-N^{2\epsilon}} N^{-\epsilon} \left(\frac{4N^{2\epsilon}}{2n+1}\right)^{\frac{2n+1}{2}}$$

$$\Rightarrow N^{\epsilon+\frac{1}{2}-\alpha} = e^{-N^{2\epsilon}} \left(\frac{4N^{2\epsilon}}{2n+1}\right)^{\frac{2n+1}{2}} \Rightarrow \left(\epsilon + \frac{1}{2} - \alpha\right) \ln N \approx -N^{2\epsilon} - n \ln\left(\frac{n}{N^{2\epsilon}}\right)$$

$$\Rightarrow \frac{n}{N^{2\epsilon}} \ln\left(\frac{n}{N^{2\epsilon}}\right) = \left(\alpha - \epsilon - \frac{1}{2}\right) \frac{\ln N}{N^{2\epsilon}} - 1. \tag{A8}$$

Let $y = \frac{n}{N^{2\epsilon}}$. For $\alpha > \epsilon + \frac{1}{2}$, $y \ln y \approx \mathcal{O}(\frac{\ln N}{N^{2\epsilon}})$ and $0 < y < 1$ as $1 \leqslant n < N^{2\epsilon}$, where $-e^{-1} \leqslant y \ln y < 0$ ($y \ln y = -e^{-1}$ for $y = y_0 \approx 0.36788$). Consider the domain $[n, n + \delta_n]$ within which $y - y_0 \approx y_0 \ln y_0$, i.e.,

$$y - y_0 = \frac{n+\delta_n}{N^{2\epsilon}} - \frac{n}{N^{2\epsilon}} = \frac{\delta_n}{N^{2\epsilon}} \approx \frac{\ln N}{N^{2\epsilon}} \Rightarrow \delta_n \approx \ln N. \tag{A9}$$

Because $y \ln y < 0$, we also require that

$$\frac{\ln N}{N^{2\epsilon}} < 1 \Rightarrow \frac{\ln \ln N}{\ln N} < 2\epsilon, \quad \lim_{N\to\infty} \frac{\ln \ln N}{\ln N} = 0. \tag{A10}$$

However, $\frac{\ln \ln N}{\ln N}$ converges very slowly to 0, hence for finite N, we cannot consider ϵ very close to 0. Then,

$$\left(\epsilon + \frac{1}{2}\right) + \frac{(1-e^{-1})N^{2\epsilon}}{\ln N} \leqslant \alpha \leqslant \left(\epsilon + \frac{1}{2}\right) + \frac{N^{2\epsilon}}{\ln N}. \tag{A11}$$

Therefore, the left side of n_0 contributes arbitrarily small intensities, i.e., $N^{-\alpha}$ with $\alpha \gg 1$, and the corresponding singularity spectrum is

$$f(\alpha) = \frac{\ln \ln N}{\ln N} \sim 0. \tag{A12}$$

Such small intensities are well below the machine precision for a modest value of $N \sim 10^6$.

APPENDIX B: CONNECTION OF THE MEAN HAMILTONIAN TO THE β ENSEMBLE

The β ensemble consists of random real symmetric tridiagonal matrices H_β [91],

$$H_\beta(n,n) \sim \mathcal{N}(0,1),$$
$$H_\beta(n,n+1) = y_n, \quad \text{such that } \sqrt{2}y_n \sim \chi_{n\beta}, \tag{B1}$$

where $\mathcal{N}(\mu, \sigma^2)$ is the Gaussian distribution with mean μ and variance σ^2, while χ_k is the χ distribution with k degrees of freedom. Then, the mth moment of y_n is $\langle y_n^m \rangle = \Gamma(\frac{n\beta+m}{2})/\Gamma(\frac{n\beta}{2})$ such that $y_n \sim \mathcal{N}(\sqrt{\frac{n\beta}{2}}, \frac{1}{4})$, provided $\beta > \frac{2}{n}$. Consequently, we can approximate the matrix H_β for $\beta > 1$ and $N \gg 1$ as

$$H_\beta \approx N^{-\frac{\gamma}{2}} \overline{H} + H_{\mathrm{A}}, \quad \beta = N^{-\gamma}, \tag{B2}$$

where $\overline{H}$ is the mean Hamiltonian defined in the main text and H_{A} is a random tridiagonal matrix with independent entries where the diagonal (off-diagonal) elements follow $\mathcal{N}(0,1)$ [$\mathcal{N}(0, \frac{1}{4})$]. Thus, H_{A} describes a 1D Anderson model with random nearest-neighbor hopping such that corresponding eigenstates are exponentially localized with $\mathcal{O}(1)$ localization length and uncorrelated energy levels as in the Poisson ensemble.

The Frobenius norms of $\overline{H}$ and H_{A} are approximately N and $\sqrt{N}$, respectively. On the other hand, the energy bandwidths of the mean Hamiltonian and H_{A} are $\mathcal{O}(\sqrt{N})$ and $\mathcal{O}(1)$, leading to mean levels spacings $\mathcal{O}(N^{-\frac{1}{2}})$ and $\mathcal{O}(N^{-1})$, respectively. Since the mean level spacing of $N^{-\frac{\gamma}{2}}\overline{H}$ is $\mathcal{O}(N^{-\frac{1+\gamma}{2}})$, first-order perturbation theory implies that the properties of the β ensemble should be well approximated by that of the mean Hamiltonian for $\gamma < -1$. This can be seen in Fig. 7, where panel (a) shows the ground state of the β ensemble with $\gamma = -1.2$ while panels (e), (i), (m), and (q) show few excited state intensities with corresponding energies denoted by x_β. We observe that irrespective of the energy, the mean Hamiltonian approximates the eigenstate intensities of the β ensemble for $\gamma < -1$ (i.e., $\beta > N$).

For $\gamma > -1$, the perturbation from H_{A} first hybridizes the energy eigenstate in the middle of the spectrum where the density of states is maximal. This is shown in Fig. 7(c), where the ground state of the β ensemble for $\gamma = -0.8$ is still well approximated by that of $\overline{H}$, while the excited states start showing small deviations [panels (g), (k), (o), and (s) in Fig. 7]. As we increase γ, the energy eigenstates of the

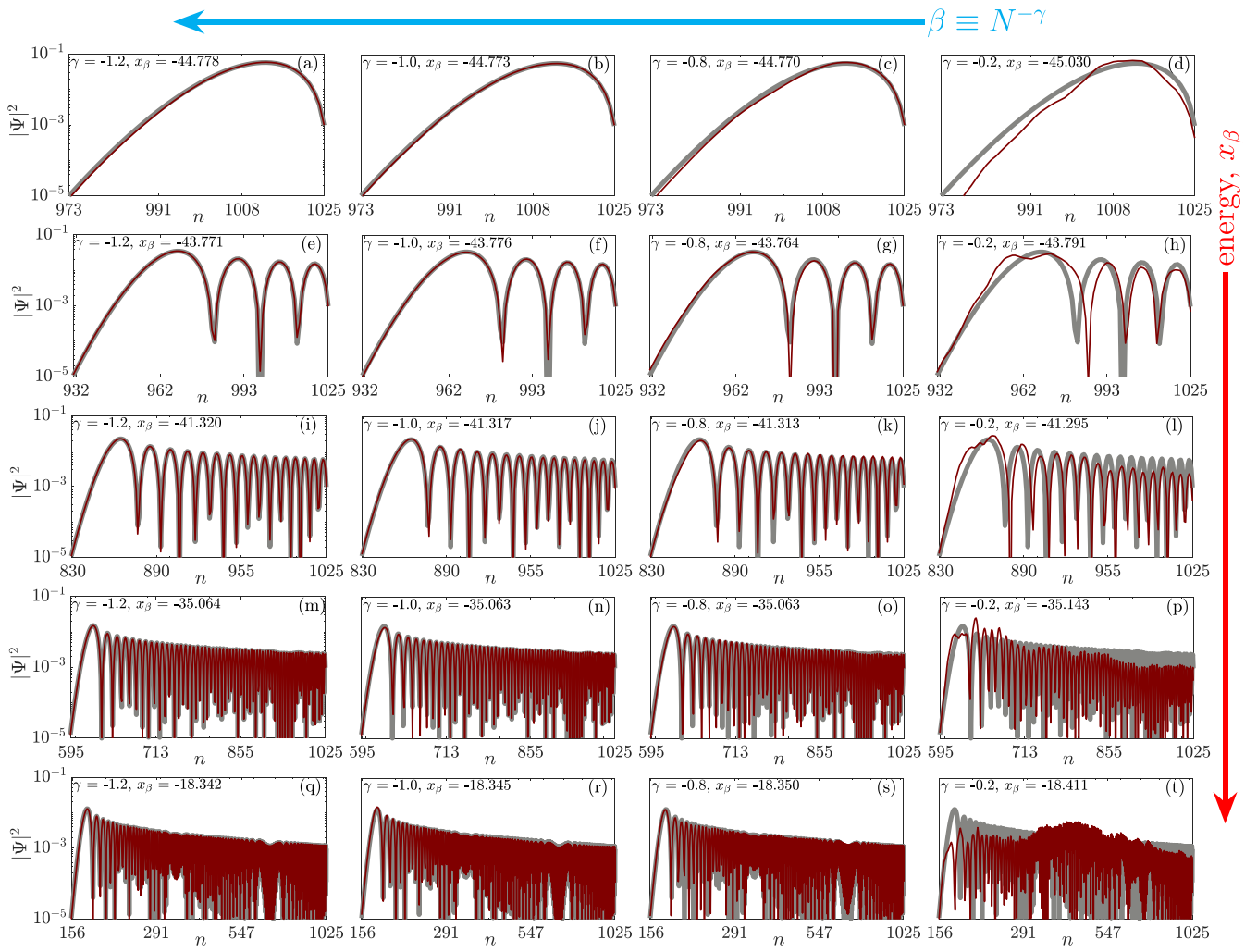


FIG. 7. Eigenstate intensities at different values of γ and energy shown via red lines for a single realization of the β ensemble with $N = 1025$. The gray curves correspond to the mean Hamiltonian, $\overline{H}$, at an equivalent energy. First, second, third, and fourth columns correspond to $\gamma = -1.2, -1, -0.8$, and -0.2, respectively. First row [panels (a)–(d)] shows the ground state of the β ensemble at various values of γ, where x_β denotes corresponding energies.

β ensemble can no longer be approximated by those of the mean Hamiltonian. This can be seen in Fig. 7, panels (d), (h), (l), (p), and (t), where we show the ground state and a few excited states of the β ensemble for $\gamma = -0.2$. Particularly, for $\gamma > 0$ (i.e., $\beta < 1$), spatially local equivalence to the 1D Anderson model allows an analytical treatment of the β ensemble [96].

The above discussion shows that the spectral structure (hence multifractality [112] of the bulk states) of the mean Hamiltonian is robust against weak global perturbations. Since the energy eigenstates of the β ensemble are well approximated by the mean Hamiltonian, we expect similar multifractal structure to be present for the bulk energy states of the β ensemble as well.

[1] D. Basko, I. Aleiner, and B. Altshuler, Metal-insulator transition in a weakly interacting many-electron system with localized single-particle states, Ann. Phys. (NY) **321**, 1126 (2006).

[2] I. V. Gornyi, A. D. Mirlin, and D. G. Polyakov, Interacting electrons in disordered wires: Anderson localization and low-T transport, Phys. Rev. Lett. **95**, 206603 (2005).

[3] A. Pal and D. A. Huse, Many-body localization phase transition, Phys. Rev. B **82**, 174411 (2010).

[4] F. Alet and N. Laflorencie, Many-body localization: An introduction and selected topics, C. R. Phys. **19**, 498 (2018).

[5] D. A. Abanin, E. Altman, I. Bloch, and M. Serbyn, *Colloquium*: Many-body localization, thermalization, and entanglement, Rev. Mod. Phys. **91**, 021001 (2019).

[6] E. J. Torres-Herrera and L. F. Santos, Effects of the interplay between initial state and Hamiltonian on the thermalization of isolated quantum many-body systems, Phys. Rev. E **88**, 042121 (2013).

[7] E. J. Torres-Herrera and L. F. Santos, Dynamics at the many-body localization transition, Phys. Rev. B **92**, 014208 (2015).

[8] P. Sierant, M. Lewenstein, A. Scardicchio, L. Vidmar, and J. Zakrzewski, Many-body localization in the age of classical computing, Rep. Prog. Phys. **88**, 026502 (2025).

[9] D. J. Luitz, N. Laflorencie, and F. Alet, Many-body localization edge in the random-field Heisenberg chain, Phys. Rev. B **91**, 081103(R) (2015).

[10] N. Macé, F. Alet, and N. Laflorencie, Multifractal scalings across the many-body localization transition, Phys. Rev. Lett. **123**, 180601 (2019).

[11] K. S. Tikhonov and A. D. Mirlin, Many-body localization transition with power-law interactions: Statistics of eigenstates, Phys. Rev. B **97**, 214205 (2018).

[12] G. De Tomasi, I. M. Khaymovich, F. Pollmann, and S. Warzel, Rare thermal bubbles at the many-body localization transition from the Fock space point of view, Phys. Rev. B **104**, 024202 (2021).

[13] A. Solórzano, L. F. Santos, and E. J. Torres-Herrera, Multifractality and self-averaging at the many-body localization transition, Phys. Rev. Res. **3**, L032030 (2021).

[14] M. A. Bastarrachea-Magnani, D. Villaseñor, J. Chávez-Carlos, S. Lerma-Hernández, L. F. Santos, and J. G. Hirsch, Quantum multifractality as a probe of phase space in the Dicke model, Phys. Rev. E **109**, 034202 (2024).

[15] P. Sierant and X. Turkeshi, Universal behavior beyond multifractality of wave functions at measurement-induced phase transitions, Phys. Rev. Lett. **128**, 130605 (2022).

[16] P. W. Anderson, Absence of diffusion in certain random lattices, Phys. Rev. **109**, 1492 (1958).

[17] F. Evers and A. D. Mirlin, Anderson transitions, Rev. Mod. Phys. **80**, 1355 (2008).

[18] A. D. Mirlin, Y. V. Fyodorov, F.-M. Dittes, J. Quezada, and T. H. Seligman, Transition from localized to extended eigenstates in the ensemble of power-law random banded matrices, Phys. Rev. E **54**, 3221 (1996).

[19] X. Cai, L.-J. Lang, S. Chen, and Y. Wang, Topological superconductor to Anderson localization transition in one-dimensional incommensurate lattices, Phys. Rev. Lett. **110**, 176403 (2013).

[20] W. DeGottardi, D. Sen, and S. Vishveshwara, Majorana fermions in superconducting 1D systems having periodic, quasiperiodic, and disordered potentials, Phys. Rev. Lett. **110**, 146404 (2013).

[21] J. Wang, X.-J. Liu, G. Xianlong, and H. Hu, Phase diagram of a non-Abelian Aubry-André-Harper model with p-wave superfluidity, Phys. Rev. B **93**, 104504 (2016).

[22] N. Rosenzweig and C. E. Porter, "Repulsion of energy levels" in complex atomic spectra, Phys. Rev. **120**, 1698 (1960).

[23] V. E. Kravtsov, I. M. Khaymovich, E. Cuevas, and M. Amini, A random matrix model with localization and ergodic transitions, New J. Phys. **17**, 122002 (2015).

[24] D. Facoetti, P. Vivo, and G. Biroli, From non-ergodic eigenvectors to local resolvent statistics and back: A random matrix perspective, Europhys. Lett. **115**, 47003 (2016).

[25] K. Truong and A. Ossipov, Eigenvectors under a generic perturbation: Non-perturbative results from the random matrix approach, Europhys. Lett. **116**, 37002 (2016).

[26] P. von Soosten and S. Warzel, Non-ergodic delocalization in the Rosenzweig-Porter model, Lett. Math. Phys. **109**, 905 (2019).

[27] C. Monthus, Multifractality of eigenstates in the delocalized non-ergodic phase of some random matrix models: Wigner-Weisskopf approach, J. Phys. A: Math. Theor. **50**, 295101 (2017).

[28] E. Bogomolny and M. Sieber, Eigenfunction distribution for the Rosenzweig-Porter model, Phys. Rev. E **98**, 032139 (2018).

[29] V. E. Kravtsov, I. M. Khaymovich, B. L. Altshuler, and L. B. Ioffe, Localization transition on the random regular graph as an unstable tricritical point in a log-normal Rosenzweig-Porter random matrix ensemble, arXiv:2002.02979.

[30] I. M. Khaymovich, V. E. Kravtsov, B. L. Altshuler, and L. B. Ioffe, Fragile extended phases in the log-normal Rosenzweig-Porter model, Phys. Rev. Res. **2**, 043346 (2020).

[31] G. Biroli and M. Tarzia, Lévy-Rosenzweig-Porter random matrix ensemble, Phys. Rev. B **103**, 104205 (2021).

[32] I. M. Khaymovich and V. E. Kravtsov, Dynamical phases in a "multifractal" Rosenzweig-Porter model, SciPost Phys. **11**, 045 (2021).

[33] W. Buijsman and Y. B. Lev, Circular Rosenzweig-Porter random matrix ensemble, SciPost Phys. **12**, 082 (2022).

[34] D. Venturelli, L. F. Cugliandolo, G. Schehr, and M. Tarzia, Replica approach to the generalized Rosenzweig-Porter model, SciPost Phys. **14**, 110 (2023).

[35] G. De Tomasi and I. M. Khaymovich, Non-Hermitian Rosenzweig-Porter random-matrix ensemble: Obstruction to the fractal phase, Phys. Rev. B **106**, 094204 (2022).

[36] M. Sarkar, R. Ghosh, and I. M. Khaymovich, Tuning the phase diagram of a Rosenzweig-Porter model with fractal disorder, Phys. Rev. B **108**, L060203 (2023).

[37] A. K. Das and A. Ghosh, Eigenvalue statistics for generalized symmetric and Hermitian matrices, J. Phys. A: Math. Theor. **52**, 395001 (2019).

[38] A. K. Das and A. Ghosh, Chaos due to symmetry-breaking in deformed Poisson ensemble, J. Stat. Mech. (2022) 063101.

[39] A. K. Das and A. Ghosh, Dynamical signatures of chaos to integrability crossover in 2×2 generalized random matrix ensembles, J. Phys. A: Math. Theor. **56**, 495003 (2023).

[40] I. Vallejo-Fabila, A. K. Das, D. A. Zarate-Herrada, A. S. Matsoukas-Roubeas, E. J. Torres-Herrera, and L. F. Santos, Reducing dynamical fluctuations and enforcing self-averaging by opening many-body quantum systems, Phys. Rev. B **110**, 075138 (2024).

[41] A. Kutlin and I. M. Khaymovich, Anatomy of the eigenstates distribution: A quest for a genuine multifractality, SciPost Phys. **16**, 008 (2024).

[42] M. V. Feigel'man, L. B. Ioffe, V. E. Kravtsov, and E. A. Yuzbashyan, Eigenfunction fractality and pseudogap state near the superconductor-insulator transition, Phys. Rev. Lett. **98**, 027001 (2007).

[43] M. Feigel'man, L. Ioffe, V. Kravtsov, and E. Cuevas, Fractal superconductivity near localization threshold, Ann. Phys. (NY) **325**, 1390 (2010).

[44] I. S. Burmistrov, I. V. Gornyi, and A. D. Mirlin, Enhancement of the critical temperature of superconductors by Anderson localization, Phys. Rev. Lett. **108**, 017002 (2012).

[45] A. P. Petrović, D. Ansermet, D. Chernyshov, M. Hoesch, D. Salloum, P. Gougeon, M. Potel, L. Boeri, and C. Panagopoulos, A disorder-enhanced quasi-one-dimensional superconductor, Nat. Commun. **7**, 12262 (2016).

[46] B. Sacépé, M. Feigel'man, and T. M. Klapwijk, Quantum breakdown of superconductivity in low-dimensional materials, Nat. Phys. **16**, 734 (2020).

[47] V. N. Smelyanskiy, K. Kechedzhi, S. Boixo, S. V. Isakov, H. Neven, and B. Altshuler, Nonergodic delocalized states for efficient population transfer within a narrow band of the energy landscape, Phys. Rev. X **10**, 011017 (2020).

[48] K. Kechedzhi, V. Smelyanskiy, J. R. McClean, V. S. Denchev, M. Mohseni, S. Isakov, S. Boixo, B. Altshuler, and H. Neven, Efficient population transfer via non-ergodic extended states in quantum spin glass, arXiv:1807.04792.

[49] T. Micklitz, F. Monteiro, and A. Altland, Nonergodic extended states in the Sachdev-Ye-Kitaev model, Phys. Rev. Lett. **123**, 125701 (2019).

[50] A. K. H. Wang, Many-body localization in a modified SYK model (2019), http://meetings.aps.org/Meeting/MAR19/Session/H06.6.

[51] A. Kamenev, Many-body localization in SYK models (2018), http://eugenekanzieper.faculty.hit.ac.il/yad8/2018/pages/schedule-abstracts.html.

[52] L. F. Cugliandolo, G. Schehr, M. Tarzia, and D. Venturelli, Multifractal phase in the weighted adjacency matrices of random Erdös-Rényi graphs, Phys. Rev. B **110**, 174202 (2024).

[53] J. D. Silva and F. L. Metz, Analytic solution of the resolvent equations for heterogeneous random graphs: Spectral and localization properties, J. Phys.: Complexity **3**, 045012 (2022).

[54] D. Tapias and P. Sollich, Multifractality and statistical localization in highly heterogeneous random networks, Europhys. Lett. **144**, 41001 (2023).

[55] J. D. da Silva, D. Tapias, P. Sollich, and F. L. Metz, Spectral properties, localization transition and multifractal eigenvectors of the Laplacian on heterogeneous networks, SciPost Phys. **18**, 047 (2025).

[56] W. Tang and I. M. Khaymovich, Non-ergodic delocalized phase with Poisson level statistics, Quantum **6**, 733 (2022).

[57] V. R. Motamarri, A. S. Gorsky, and I. M. Khaymovich, Localization and fractality in disordered Russian doll model, SciPost Phys. **13**, 117 (2022).

[58] A. Lakshminarayan, S. Tomsovic, O. Bohigas, and S. N. Majumdar, Extreme statistics of complex random and quantum chaotic states, Phys. Rev. Lett. **100**, 044103 (2008).

[59] L. S. Levitov, Absence of localization of vibrational modes due to dipole-dipole interaction, Europhys. Lett. **9**, 83 (1989).

[60] L. S. Levitov, Delocalization of vibrational modes caused by electric dipole interaction, Phys. Rev. Lett. **64**, 547 (1990).

[61] A. D. Mirlin and F. Evers, Multifractality and critical fluctuations at the Anderson transition, Phys. Rev. B **62**, 7920 (2000).

[62] A. L. Burin and L. A. Maksimov, Localization and delocalization of particles in disordered lattice with tunneling amplitude with R^{-3} decay, Pis'ma Zh. Eksp. Teor. Fiz. **50**, 304 (1989) [Sov. Phys. JETP Lett. **50**, 338 (1989)].

[63] A Rodríguez, V. A. Malyshev, and F. Dominguez-Adame, Quantum diffusion and lack of universal one-parameter scaling in one-dimensional disordered lattices with long-range coupling, J. Phys. A: Math. Gen. **33**, L161 (2000).

[64] D. B. Balagurov, V. A. Malyshev, and F. Dominiquez-Adame, Phase coherence in tight-binding models with nonrandom long-range hopping, Phys. Rev. B **69**, 104204 (2004).

[65] F. A. B. F. de Moura, A. V. Malyshev, M. L. Lyra, V. A. Malyshev, and F. Dominguez-Adame, Localization properties of a one-dimensional tight-binding model with nonrandom long-range intersite interactions, Phys. Rev. B **71**, 174203 (2005).

[66] X. Deng, V. E. Kravtsov, G. V. Shlyapnikov, and L. Santos, Duality in power-law localization in disordered one-dimensional systems, Phys. Rev. Lett. **120**, 110602 (2018).

[67] X. Deng, A. L. Burin, and I. M. Khaymovich, Anisotropy-mediated reentrant localization, SciPost Phys. **13**, 116 (2022).

[68] J. T. Cantin, T. Xu, and R. V. Krems, Effect of the anisotropy of long-range hopping on localization in three-dimensional lattices, Phys. Rev. B **98**, 014204 (2018).

[69] A. Krishna and R. N. Bhatt, Effect of Hilbert space truncation on Anderson localization, Phys. Rev. B **97**, 174205 (2018).

[70] P. A. Nosov, I. M. Khaymovich, and V. E. Kravtsov, Correlation-induced localization, Phys. Rev. B **99**, 104203 (2019).

[71] P. A. Nosov and I. M. Khaymovich, Robustness of delocalization to the inclusion of soft constraints in long-range random models, Phys. Rev. B **99**, 224208 (2019).

[72] A. G. Kutlin and I. M. Khaymovich, Renormalization to localization without a small parameter, SciPost Phys. **8**, 049 (2020).

[73] A. G. Kutlin and I. M. Khaymovich, Emergent fractal phase in energy stratified random models, SciPost Phys. **11**, 101 (2021).

[74] E. Bogomolny and M. Sieber, Power-law random banded matrices and ultrametric matrices: Eigenvector distribution in the intermediate regime, Phys. Rev. E **98**, 042116 (2018).

[75] P. von Soosten and S. Warzel, The phase transition in the ultrametric ensemble and local stability of Dyson Brownian motion, Electron. J. Probab. **23**, 1 (2018).

[76] G. De Tomasi and I. M. Khaymovich, Non-Hermiticity induces localization: Good and bad resonances in power-law random banded matrices, Phys. Rev. B **108**, L180202 (2023).

[77] D. C. Herbert and R. Jones, Localized states in disordered systems, J. Phys. C **4**, 1145 (1971).

[78] D. J. Thouless, A relation between the density of states and range of localization for one dimensional random systems, J. Phys. C **5**, 77 (1972).

[79] E. J. Torres-Herrera, J. A. Méndez-Bermúdez, and L. F. Santos, Level repulsion and dynamics in the finite one-dimensional Anderson model, Phys. Rev. E **100**, 022142 (2019).

[80] W. P. Su, J. R. Schrieffer, and A. J. Heeger, Solitons in polyacetylene, Phys. Rev. Lett. **42**, 1698 (1979).

[81] R. Chaunsali, H. Xu, J. Yang, P. G. Kevrekidis, and G. Theocharis, Stability of topological edge states under strong nonlinear effects, Phys. Rev. B **103**, 024106 (2021).

[82] C. Albanese, M. Christandl, N. Datta, and A. Ekert, Mirror inversion of quantum states in linear registers, Phys. Rev. Lett. **93**, 230502 (2004).

[83] M. Christandl, N. Datta, A. Ekert, and A. J. Landahl, Perfect state transfer in quantum spin networks, Phys. Rev. Lett. **92**, 187902 (2004).

[84] T. Shi, Y. Li, Z. Song, and C.-P. Sun, Quantum-state transfer via the ferromagnetic chain in a spatially modulated field, Phys. Rev. A **71**, 032309 (2005).

[85] G. M. Nikolopoulos, D. Petrosyan, and P. Lambropoulos, Electron wavepacket propagation in a chain of coupled quantum dots, J. Phys.: Condens. Matter **16**, 4991 (2004).

[86] R. J. Chapman, M. Santandrea, Z. Huang, G. Corrielli, A. Crespi, M.-H. Yung, R. Osellame, and A. Peruzzo, Experimental perfect state transfer of an entangled photonic qubit, Nat. Commun. **7**, 11339 (2016).

[87] C. Lanczos, An iteration method for the solution of the eigenvalue problem of linear differential and integral operators, J. Res. Natl. Bur. Stand. B **45**, 255 (1950).

[88] W. E. Arnoldi, The principle of minimized iterations in the solution of the matrix eigenvalue problem, Q. Appl. Math. **9**, 17 (1951).

[89] V. S. Viswanath and G. Müller, *The Recursion Method: Application to Many-Body Dynamics* (Springer, Berlin, Heidelberg, 1994).

[90] D. E. Parker, X. Cao, A. Avdoshkin, T. Scaffidi, and E. Altman, A universal operator growth hypothesis, Phys. Rev. X **9**, 041017 (2019).

[91] I. Dumitriu and A. Edelman, Matrix models for beta ensembles, J. Math. Phys. **43**, 5830 (2002).

[92] V. Balasubramanian, J. M. Magan, and Q. Wu, A tale of two Hungarians: Tridiagonalizing random matrices, arXiv:2208.08452.

[93] M. Mehta, *Random Matrices* (Elsevier Science, Amsterdam, Netherlands, 2004).

[94] A. K. Das, A. Ghosh, and I. M. Khaymovich, Robust nonergodicity of the ground states in the β ensemble, Phys. Rev. B **109**, 064206 (2024).

[95] A. K. Das and A. Ghosh, Nonergodic extended states in the β ensemble, Phys. Rev. E **105**, 054121 (2022).

[96] A. K. Das, A. Ghosh, and I. M. Khaymovich, Absence of mobility edge in short-range uncorrelated disordered model: Coexistence of localized and extended states, Phys. Rev. Lett. **131**, 166401 (2023).

[97] A. Relaño, L. Muñoz, J. Retamosa, E. Faleiro, and R. A. Molina, Power-spectrum characterization of the continuous Gaussian ensemble, Phys. Rev. E **77**, 031103 (2008).

[98] B. Roy, A. K. Das, A. Ghosh, and I. M. Khaymovich, Anomalous energy correlations and spectral form factor in the nonergodic phase of the β-ensemble, arXiv:2506.15283.

[99] J. Breuer, P. J. Forrester, and U. Smilansky, Random discrete Schrödinger operators from random matrix theory, J. Phys. A: Math. Theor. **40**, F161 (2007).

[100] J. Breuer, Spectral and dynamical properties of certain random Jacobi matrices with growing parameters, Trans. Am. Math. Soc. **362**, 3161 (2010).

[101] G. Lambert and E. Paquette, Strong approximation of Gaussian β ensemble characteristic polynomials: The hyperbolic regime, Ann. Appl. Probab. **33**, 549 (2023).

[102] G. Lambert and E. Paquette, Strong approximation of Gaussian β-ensemble characteristic polynomials: The edge regime and the stochastic Airy function, arXiv:2009.05003.

[103] D. J. Griffiths and D. F. Schroeter, *Introduction to Quantum Mechanics* (Cambridge University Press, Cambridge, England, 2018).

[104] G. Szegö, *Orthogonal Polynomials* (American Mathematical Society, Providence, RI, 1959).

[105] C. M. Soukoulis and E. N. Economou, Fractal character of eigenstates in disordered systems, Phys. Rev. Lett. **52**, 565 (1984).

[106] H. G. E. Hentschel and I. Procaccia, The infinite number of generalized dimensions of fractals and strange attractors, Phys. D (Amsterdam, Neth.) **8**, 435 (1983).

[107] A. Bäcker, M. Haque, and I. M. Khaymovich, Multifractal dimensions for random matrices, chaotic quantum maps, and many-body systems, Phys. Rev. E **100**, 032117 (2019).

[108] A. Vikram and V. Galitski, Dynamical quantum ergodicity from energy level statistics, Phys. Rev. Res. **5**, 033126 (2023).

[109] Y. V. Fyodorov and O. Giraud, High values of disorder-generated multifractals and logarithmically correlated processes, Chaos Solitons Fract. **74**, 15 (2015).

[110] A. Chhabra and R. V. Jensen, Direct determination of the f(α) singularity spectrum, Phys. Rev. Lett. **62**, 1327 (1989).

[111] D. Dominici, Asymptotic analysis of the Hermite polynomials from their differential-difference equation, arXiv:math/0601078.

[112] Y. Y. Atas and E. Bogomolny, Multifractality of eigenfunctions in spin chains, Phys. Rev. E **86**, 021104 (2012).